九州大学学術情報リポジトリ
Kyushu University Institutional Repository

An Analytical Study on the Pull-Out Strength of Anchor Bolts Embedded in Concrete Members by SPH Method

Lu, Chi
Department of Civil Engineering, Faculty of Engineering, Kyushu University

Sonoda, Yoshimi
Department of Civil Engineering, Faculty of Engineering, Kyushu University

https://hdl.handle.net/2324/4793218

出版情報：Applied Sciences. 11 (18), pp.8526-, 2021-09-14. MDPI
バージョン：
権利関係：(c) 2021 by the authors.This article is an open access article distributed under the terms and conditions of the Creative Commons Attribution (CC BY) license.

KYUSHU UNIVERSITY

applied sciences

MDPI

Article

An Analytical Study on the Pull-Out Strength of Anchor Bolts Embedded in Concrete Members by SPH Method

Chi Lu * and Yoshimi Sonoda

Department of Civil Engineering, Kyushu University, Motooka, Nishi-ku, Fukuoka 819-0395, Japan; sonoda@doc.kyushu-u.ac.jp
* Correspondence: luchi@doc.kyushu-u.ac.jp

Abstract: As an important method for connecting structural members, anchor bolts have been installed in many situations. Therefore, accurate evaluation of the pull-out strength of anchor bolts has always been an important issue, considering the complicated actual installation conditions and the problem of aging deterioration of the structural members. In general, the patterns of pull-out failure of anchor bolts can be classified into three types: adhesion failure, cone failure, and bolt break. However, it sometimes shows a mixed fracture pattern, and it is not always easy to predict the accurate pull-out strength. In this study, we attempted to evaluate the pull-out strength of anchor bolts under various installation conditions using SPH, which can analyze the crack growth process in the concrete. In particular, the anchor bolt-concrete interface model was introduced to SPH analysis in order to consider the bond failure, and it was confirmed that various failure patterns and the load capacity could be predicted by proposed SPH method. After that, the influence of several parameters, such as bond stress limit, anchor bolt diameter, and the anchor bolt embedment depth on the failure patterns and the load capacity, were investigated by numerical calculation. Furthermore, several useful suggestions on the pull-out strength of anchor bolts under improper installation conditions, such as the ends of members for the purpose of seismic retrofitting, are presented.

Keywords: concrete; anchor bolt; pull-out strength; SPH method

check for updates

Citation: Lu, C.; Sonoda, Y. An Analytical Study on the Pull-Out Strength of Anchor Bolts Embedded in Concrete Members by SPH Method. *Appl. Sci.* **2021**, *11*, 8526. https://doi.org/10.3390/app11188526

Academic Editor: Maria Favvata

Received: 14 August 2021
Accepted: 10 September 2021
Published: 14 September 2021

Publisher's Note: MDPI stays neutral with regard to jurisdictional claims in published maps and institutional affiliations.

Copyright: © 2021 by the authors. Licensee MDPI, Basel, Switzerland. This article is an open access article distributed under the terms and conditions of the Creative Commons Attribution (CC BY) license (https://creativecommons.org/licenses/by/4.0/).

1. Introduction

When constructing a structure in the civil engineering field, a joining method that has structural continuity between concrete members and other members (reliable stress transmission) is very important, and joining with anchor bolts is one of the typical methods not only in new structures but also in existing structures. In addition, anchor bolts are used to connect the seismic retrofitting members, such as bridge restrainers [1] and shear walls, to existing concrete structures. Anchor bolts are also applied in railway sleepers [2], modular wall constructions [3], tunnel roofs [4], and nuclear-related facilities [5], and they are expected to continue to be used in the future. However, only a simple evaluation has been made for the ultimate strength when a pull-out load is applied to the anchor bolt. Therefore, there is a concern that the pull-out strength of bolts will be significantly reduced due to improper installation conditions and the aging deterioration of concrete materials.

In general, fracture modes of anchor bolts subjected to a pull-out load are mainly classified into bolt fracture, concrete body fracture, and bond fracture. Table 1 shows the typical fracture modes assumed when designing anchor bolts and shows the equations for calculating the pull-out strength of each fracture type. Basically, it is designed using the pull-out strength of the fracture mode, which has the lowest strength among the assumed these fracture modes shown in Table 1.

However, when installing new anchor bolts in an existing concrete structure, it may be difficult to secure sufficient anchor embedding depth and spacing between adjacent anchor bolts, depending on the arrangement of existing reinforcing bars inside. Furthermore, it is

well known that the actual fracture mode of anchor bolt joint cannot be clearly classified into three types, and that a combined fracture mode in which cone fracture and adhesive fracture might occur depending on the installation conditions. For example, Figure 1a [6] shows the fracture of an anchor bolt in the pull-out test conducted by the authors, and a clear combined fracture mode in which cone fracture and adhesion fracture are mixed is obtained. Thus, a simple evaluation based on the strength comparison of each mode shown in Table 1 may not be applicable. Therefore, it is very important to establish a method that can predict the accurate fracture mode and pull-out strength of anchor bolts with various material properties, structural specifications, and loading conditions.

Table 1. Typical fracture patterns of anchor bolts and corresponding strength.

Anchor Bolt Fracture	Cone Fracture	Bond Fracture
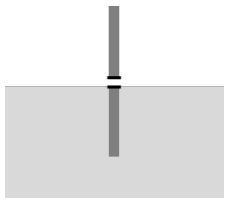	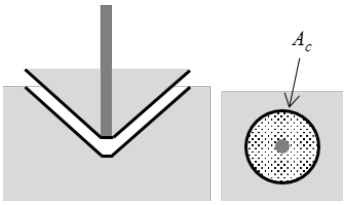	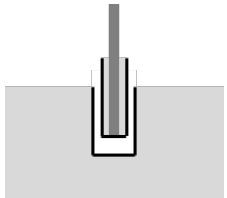
$T = \sigma_y a_0$	$T = 0.23\sqrt{\sigma_B} A_c$	$T = \tau \pi d_a l_e$

T: Maximum pull-out force, σ_y: Steel yield strength; a_0: Anchor bolt nominal cross-section area, σ_B: Concrete compressive strength; τ: Maximum bond stress, d_a: Anchor bolt nominal diameter, l_e: embedment depth.

In addition, when installing anchor bolts in an existing concrete structure where complex rebars arrangements are already embedded inside, it is often difficult to secure sufficient embedding depth, anchor bolt spacing, and distance from the edge of the structural member depending on the position of the existing internal reinforcing bars. Figure 1b shows an example of damage to an anchor bolt joint with a bridge collapse prevention device attached by the earthquake force. This accident is a typical fracture due to the insufficient distance from the edge, and this installation situation is not included in Table 1 either. Thus, in order to design and apply anchor bolts to structure members with sufficient structural safety, the installation situations and the damage patterns which are not included in the existing specifications are also needed to be taken into consideration. In this study, minimum allowable embedding depth, minimum bolt spacing, and minimum distance from the edge of structural member were evaluated, respectively, and proper reinforcement for the lack of distance from the edge of structural member was considered.

(**a**) (**b**)

Figure 1. Actual fracture patterns in experiment and structural members. (**a**) Complex fracture pattern shown in anchor bolt pull-out experiment [6]. (**b**) Actual anchor bolt fracture due to the insufficient distance from the edge of the concrete abutment.

Under these backgrounds, many researchers have already conducted the research on the pull-out fracture of anchor bolts. For example, there are experimental studies [5,7–9],

some of them focusing on the damage of the base concrete [10,11], and others focusing on the bond fracture between concrete and anchor bolt [12,13], and studies focusing on the long-term strength against aging performance [14].

On the other hand, there are many analytical studies using numerical method and not only general FE method [15,16] but also new mesh-free methods, such as Galerkin method [17], and peridynamic theory [18]. Furthermore, there are studies that use neural networks to predict the strength of anchor bolts from installation conditions [19].

In this study, we will analyze the effect of basic factors (embedded depth, bolt diameter, etc.) on the load bearing performance of anchor bolts using SPH (Smoothed Particle Hydrodynamics) [20], referring to the existing research results. The advantage of using the SPH method, which is one of the mesh-free methods, is that, unlike the ordinary finite element method, the particles are not constrained by the conditions of displacement field, and fracture between particles is easily reproduced [21,22].

With reference to these research results, we will propose an evaluation method that can accurately predict the ultimate strength of anchor bolts and simulate the fracture process of pulling out anchor bolts. Specifically, we will introduce an analysis model that can accurately produce the crack development during the pull-out process and evaluate concrete fracture, bolt fracture, and steel-concrete bond fracture in the SPH method.

The fracture mode obtained by the analysis was compared with the experimental results to reproduce the pull-out fracture of the anchor bolt under various installation conditions. Considering the actual installation of the anchor bolts on an existing structure where rebars are already embedded inside, there may be certain restriction on the anchor bolt embedment depth, the interval between anchor bolts, and the distance from the free-end of the structure members. Thus, these are chosen as the input parameter in the analysis to evaluate the performance of anchor bolts under inappropriate condition. Then, we presented several useful suggestions on the pull-out strength of anchor bolts under improper installation conditions. Finally, considering the installation conditions shown in the Figure 1b, the attempt of applying PCM material [23,24] as a reinforcement is performed, and several suggestions are made when using such kind of reinforcement.

2. Analysis Method in This Study

In this study, SPH method, which is one of the most popular mesh-free methods, is adopted in order to analyze local fracture phenomena of concrete which are difficult to simulate by FEM. The physical quantity of each particle is evaluated by the weighted average of the adjacent particles using the kernel function, as shown in Figure 2, and the basic equation of the SPH method is written as Equation (1).

$$< f(x_i) >= \int_{\Omega} f(x_i) W(x_i - x_j, h)\, dx_j, \tag{1}$$

where W is the kernel function, h is the smoothing length, terms inside angel bracket are SPH approximations, Ω is the integral area within the support domain, and x_i, x_j are the position of particle i and j.

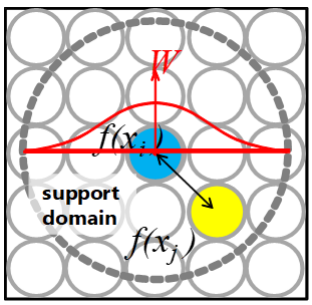

Figure 2. Influence domain of SPH particles (kernel function).

The smoothing length h is very important in SPH analysis. If it is too large, the accuracy of the analysis would be affected due to the smoothed-out details and local properties; on the other hand, if it is too small, the number of particles within smoothing domain may not be enough to calculate accurate response of particles [25]. Thus, in this study, an adaptive smooth length h_a is utilized. Since SPH method is to calculate weighted average values within the smoothing length, an adaptive smoothing length is better for the calculation of local deformation and stress concentration. The adaptive smoothing length h_a is changed during the analysis with the density of the particle, which is widely used in SPH analyses, as shown in Equation (2).

$$h_a = h_0 \left(\frac{\rho_0}{\rho_{current}} \right)^{\frac{1}{3}}, \tag{2}$$

where h_0 is the initial smoothing length, ρ_0 is the initial density of the particle, and $\rho_{current}$ is the density of particle calculated by SPH process, shown in Equation (3).

$$\rho_{current} = \sum_{j=1}^{N} m_j W_{ij}. \tag{3}$$

By the above calculation, the smoothing length h_a is decreased when the influence domain is compressed with the increase of density.

When adaptive smoothing length h_a is adopted in SPH analysis, to obey Newton's third law and conservation of momentum, the following changes are applied to the calculation of kernel function, shown in Equation (4).

$$< f(x_i) >= \int_{\Omega} f(x_i) W \left(x_i - x_j, \frac{h_i + h_j}{2} \right) dx_j. \tag{4}$$

By the above calculation, the interaction force between pairing particles by SPH analysis maintains the same.

If two particles are positioned with smaller distance than h_0 at the beginning of the analysis, we defined that the two particles are "SPH-linked", and the SPH-link between them will break when the distance between them is larger than h_a, or the particles enter the crushing state, which is explained in the next section. Damage in solids is generally unrecoverable, and solid material, such as concrete, is not able to bond together due to the decrease of distance. Thus, if two particles are not SPH-linked at the beginning of the analysis, or SPH-link breaks by concrete fracture, no SPH link will be generated, even if the distance between particles become smaller than h_a.

To calculate the bond stress between concrete and steel anchor bar, the normal direction of the contact surface $\boldsymbol{n}$ should be defined at the beginning of the numerical analysis. When the steel anchor is being pulled out, displacement $\boldsymbol{dr}$ would occur within the pair of neighboring concrete particle and steel particle, as shown in the Figure 3a. Using the normal direction and the vector of the two particles, the slip along the tangential direction $\boldsymbol{t}$ can be calculated as in Equation (5). Finally, by using the relationship between bond stress τ and slip distance $|\boldsymbol{t}|$, the bond stress can be obtained, as shown in Figure 3b and Equation (6).

$$\boldsymbol{t} = -(\boldsymbol{dr} - \boldsymbol{dr} \cdot \boldsymbol{n}), \tag{5}$$

$$\tau_{ij} = f_b(|\boldsymbol{t}|). \tag{6}$$

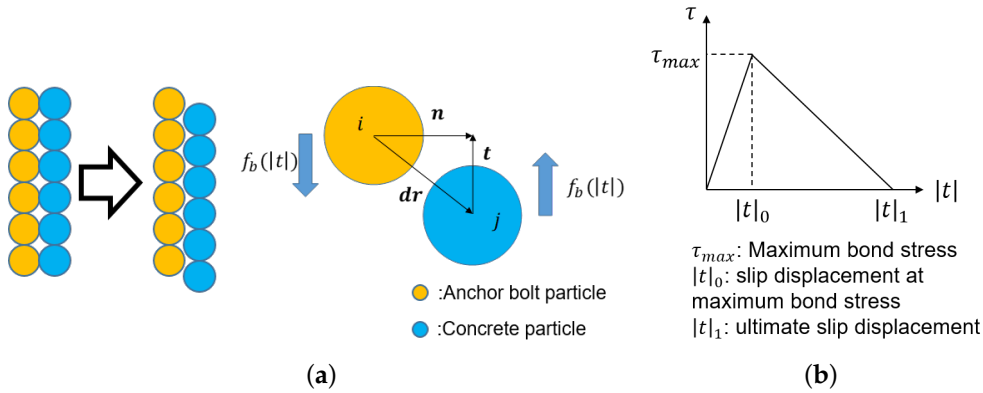

Figure 3. Calculation of bond stress. (**a**) Slip displacement between steel particle and concrete particle. (**b**) Relationship between slip displacement and bond stress abutment.

3. Overview of Crack Growth Analysis

To analyze the elasto-plastic behavior of concrete, a pressure-dependent yield function, such as Drucker-Prager's equation, is often used for the yield criteria. However, it is well known that linear Drucker-Prager's yield surface overestimates compressive strength of concrete under high hydrostatic pressure condition. Therefore, non-linear Drucker-Prager's yield function which improves linear Drucker-Prager's equation is applied in this study. Non-linear Drucker-Prager yield function applied in this research is represented by the following Equation (7).

$$f(I_1, J_2) = \sqrt{J_2} - \sqrt{\frac{\gamma^2 - \beta I_1}{3}} = 0, \tag{7}$$

where γ is $\sqrt{(f_c f_t)}$, β is $(f_c - f_t)$, I_1 is the first invariant of stress, J_2 is the second invariant of deviatoric stress, f_c is the uniaxial compressive strength, and f_t is the uniaxial tensile strength. Figure 4 shows non-linear Drucker-Prager yield surface in the $\sqrt{J_2} - I_1$ plane.

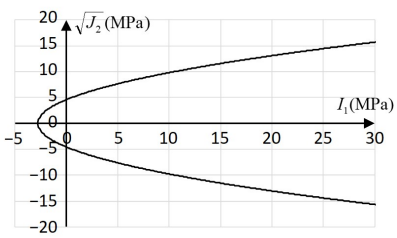

Figure 4. Nonlinear Drucker-Prager yield criterion.

Furthermore, bilinear softening of concrete is considered on the tensile stress side according to the Japanese specification [26], as shown in Figure 5, where σ_t is the tensile stress, f_t is the tensile strength of concrete, and G_F is the fracture energy of concrete determined from Japanese specifications [26].

In addition, considering the degree of damage in which the load transmission capacity in the concrete cross section decreases due to the accumulation of plastic strain, the relationship represented by the sigmoid function, as shown in Equation (8) and Figure 6, was assumed between the degree of damage and the plastic strain.

$$D_{pr} = \frac{D_{lim}}{1 + \exp[-k(\varepsilon_{pr}^p - \frac{\varepsilon_{max}^p}{2})]}, (0 \le D_{pr} \le 0.4), \tag{8}$$

where D_{pr} is the damage in the principal direction; k is the gradient adjustment constant, and $k = 300$ is applied in this study; ε^p_{pr} is the accumulated plastic strain along the principal direction; ε^p_{max} is the maximum limit of equivalent plastic strain, and $\varepsilon^p_{max} = 0.03$ is used.

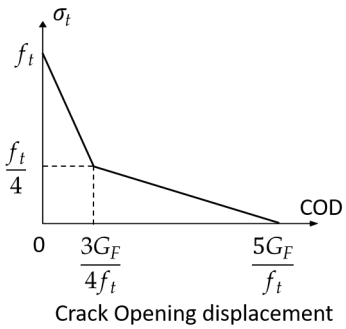

Figure 5. Tensile softening model of the concrete.

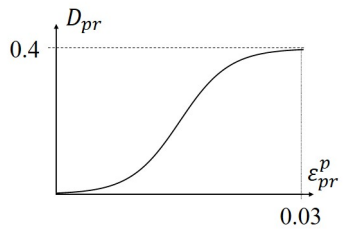

Figure 6. Damage index and principal strain relationship in the tensile side.

Compressive softening is also considered according to the Popovic's equation [27], as shown in Equations (9)–(11).

$$\sigma_{pr} = f_c \cdot \frac{n(\frac{\varepsilon_{pr}}{\varepsilon_{co}})}{(n-1) + (\frac{\varepsilon_{pr}}{\varepsilon_{co}})^n}, \tag{9}$$

$$\varepsilon_{co} = \frac{f_c}{E_c(1 - \frac{1}{n})}, \tag{10}$$

$$n = \exp(0.0256 \cdot f_c), \tag{11}$$

where f_c is the uniaxial compressive strength, ε_{pr} is the principal strain, and ε_{co}, n are parameters determined from material test results. Hardening is considered on the compression stress side, as shown in Equation (12).

$$H = \frac{d\sigma}{d\varepsilon^p}. \tag{12}$$

To obtain the the loss of elastic stiffness due to the increase of damage, the damage index in the global coordinate is calculated first with D_{pr} using Equation (13).

$$D_i = \sum_{i=1}^{3} |D_{pr} e_{i,pr}|, (i = 1, 2, 3), \tag{13}$$

where D_i is the damage index in the global coordinate, and $e_{i,pr}$ is unit vector of principal direction. This calculation process is shown in Figure 7.

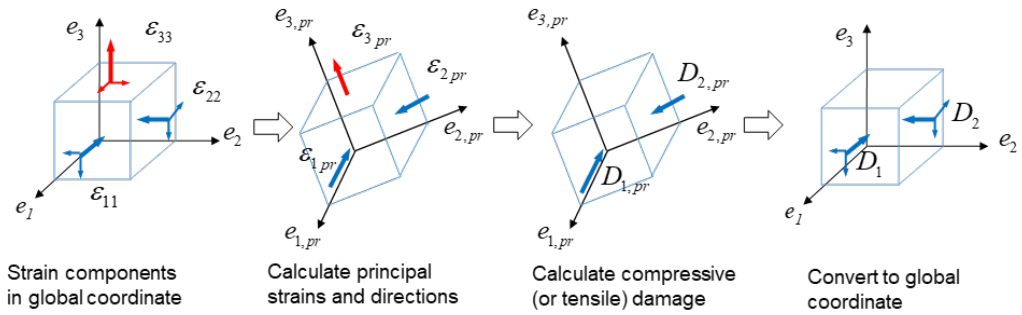

Figure 7. Damage index calculation process.

Then, the decrease ratio of elastic stiffness d_{ij} is calculated by Equation (14).

$$d_{ij} = \sqrt{(1 - D_i)(1 - D_j)}. \tag{14}$$

Finally, the elastic stiffness matrix with damage can be written as Equation (15):

$$E^e = \begin{pmatrix} (\lambda + 2\mu)d_{11} & \lambda d_{12} & \lambda d_{13} & 0 & 0 & 0 \\ \lambda d_{12} & (\lambda + 2\mu)d_{22} & \lambda d_{23} & 0 & 0 & 0 \\ \lambda d_{13} & \lambda d_{23} & (\lambda + 2\mu)d_{33} & 0 & 0 & 0 \\ 0 & 0 & 0 & 2\mu d_{12} & 0 & 0 \\ 0 & 0 & 0 & 0 & 2\mu d_{23} & 0 \\ 0 & 0 & 0 & 0 & 0 & 2\mu d_{13} \end{pmatrix}, \tag{15}$$

where $\lambda = \mu E/[(1 + \mu)(1 - 2\mu)]$, $\mu = E/[2(1 + \nu)]$, and E, ν are the Young's modulus and the Poisson's ratio, respectively.

In this study, to avoid the unrealistic volume overlap between particles, when the volumetric strain of concrete particle ε_v reaches a certain threshold value (we call it erosion limit) ε_{v_lim}, the particles are regarded as a crushing state, and stress and stiffness of the particle are assumed to be zero; however, the particle itself is not erased in order to maintain the mass conservation, and the kinetic energy and the momentum of the particle is also preserved. Based on the assumptions mentioned above, the stress-strain relationship of concrete is schematically shown in Figure 8a,b.

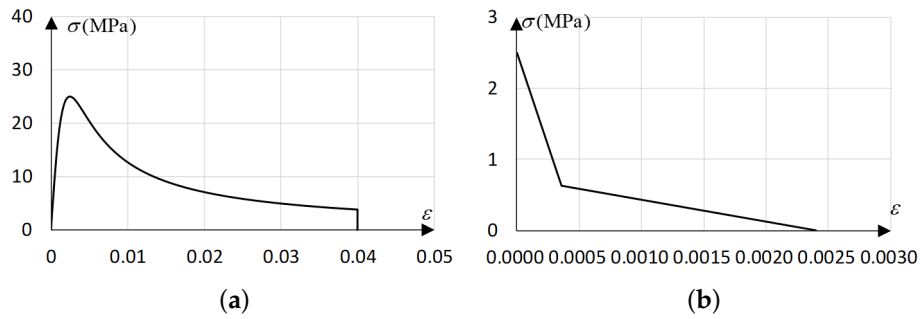

Figure 8. Uniaxial stress-strain relationship of concrete. (**a**) Compressive stress-strain relations. (**b**) Tensile stress-strain relations.

For the steel material, von Mises yield criterion is used, and strain hardening exponent is introduced to describe the hardening process. The stress-strain relationship of steel is shown in Figure 9.

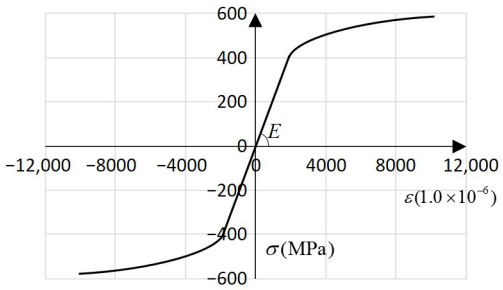

Figure 9. Stress-strain relationship of steel.

4. Anchor Bolt Pull-Out Analysis

4.1. Verification of the Proposed Method

In general, the fracture pattern when pulling out an anchor bolt embedded in a concrete member is complicated, and, as shown in experiment [6], the actual fracture pattern is often a combination of three fracture patterns (bond fracture, corn fracture, and bolt fracture). Therefore, in this study, we conducted a simulation analysis of the anchor bolt pull-out test and confirmed whether the fracture process and the pull-out strength in various fracture cases can be reproduced. The analytical model is shown in Figure 10a. Each particle in the model is 3 mm in diameter, and the total number of particles is about 200,000. An anchor bolt is embedded in the center of the concrete block. As a boundary condition, the vertical degrees of freedom of the particles (black area in the figure) at the four corners of upper surface were constrained. Table 2 shows the material constants used in the analysis.

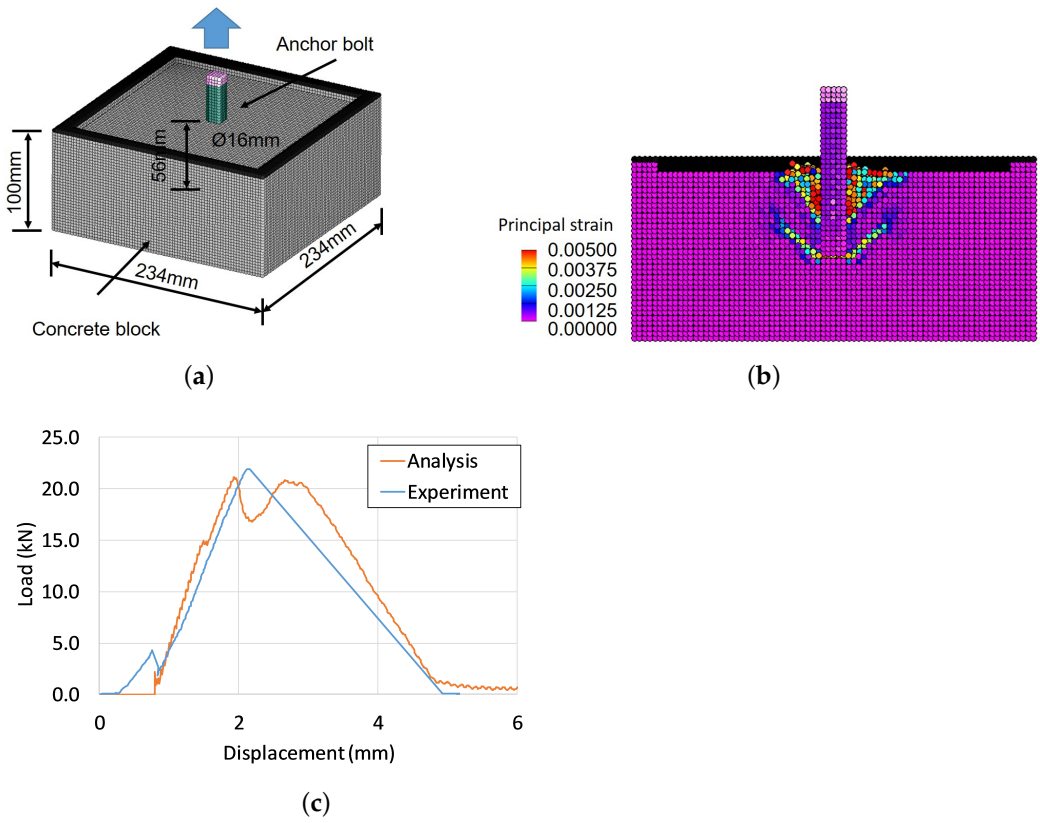

Figure 10. SPH analysis for the pull-out process in experiment [6]. (**a**) Analysis model. (**b**) Complex fracture pattern by numerical analysis. (**c**) Comparison of load-displacement relationship.

Figure 10b,c shows the final fracture pattern and the load-displacement relationship obtained from the proposed numerical analysis method. It can be found that the maximum load of the experiment is well reproduced by the numerical analysis, and the fracture pattern shown in the experiment is also reproduced by the numerical analysis. Bond fracture occurs at the lower part of the anchor, and cone fracture occurs at the upper part of the anchor. From these results, it is shown that the pull-out strength and fracture type of anchor bolts can be grasped by the proposed method.

Table 2. Material constants used in the analysis.

	Steel	Concrete
Compressive strength (MPa)	408.2	48.0
Tensile strength (MPa)	408.2	3.1
Poisson's ratio	0.30	0.20
Density (kg/m^3)	79,000	2350.0
Young's modulus (MPa)	214,000	21,430

4.2. Effect of Installation Conditions on the Fracture Mode

Next, in order to make a basic consideration of the effects of anchor bolt installation conditions (bolt diameter, embedding depth, joint strength between bolt and concrete) on pull-out strength and fracture pattern, an analysis model with the same dimensions as the specimens used in the previous study [6] was examined. An analysis model was created in which anchor bolts were embedded in the center of a concrete block, and analysis was performed by constraining the vertical displacement of the particles at the four corners, as shown in Figure 10. Here, assuming anchor bolts used to attach seismic retrofitting members to concrete blocks, we examined load-bearing performance when the embedding depth is not sufficient or when chemical adhesives with different adhesive strengths are used. Table 3 shows the material parameters used in the analysis, and Table 4 shows the condition parameters for anchor installation. In this study, 0.5 m/s was selected as the pull-out speed given to the anchor bolts according to the maximum speed level assumed for ordinary seismic wave.

Table 3. Material constants used in the analysis with different installation conditions.

	Steel	Concrete
Compressive strength (MPa)	408.2	25.0
Tensile strength (MPa)	408.2	2.5
Poisson's ratio	0.30	0.20
Density (kg/m^3)	79,000	2350.0
Young's modulus (MPa)	214,000	21,430

Table 4. Analysis cases.

Case	Maximum Bond Stress τ (MPa)	Anchor Bolt Diameter d (mm)	Anchor Bolt Embedment Depth l_e (mm)
1	8	16	48
2	12	16	48
3	16	16	48
4	12	8	48
5	12	24	48
6	12	16	32
7	12	16	64

First, the crack growth process of concrete with the increase of pull-out displacement of anchor bolts was investigated, and the adhesive stress distribution that changed, at the

same time, was analytically considered. Figure 11 show the final crack pattern of Case 1, 2, and 3, respectively. With the increase of adhesive stress limit, the fracture pattern changed from bond fracture, bond-cone combined fracture, to cone fracture.

As shown in Figure 11, there are many small cracks around the anchor bolt, and a major crack can be found at the bottom of the anchor bolt. In the case of adhesive stress limit is 16 MPa, the major crack developed to the surface of the concrete, forming a cone shaped fracture pattern.

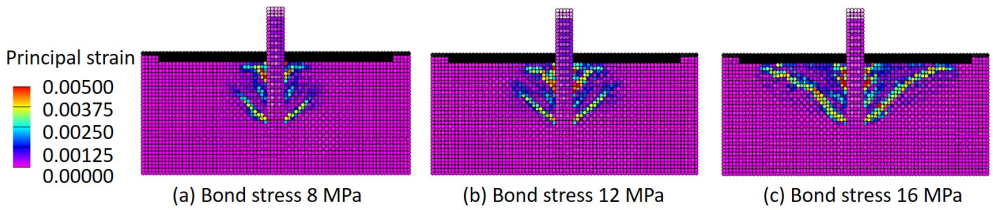

Figure 11. Effect of adhesive stress on the fracture pattern.

The bond stress development are shown in Figure 12. Due to the mechanical symmetry of the loading condition, the resulting figure shows only zoomed half of the analysis area. Focusing on the result of Figure 12a,b with the adhesive stress limit set to 8 MPa, when the pull-out displacement reaches x = 75 μm, fine cracks are seen near the anchor bolt, and the bond stress rises to about 5 MPa in the entire circumference of the anchor bolt. When pull-out displacement $x = 225$ μm, a major crack that could lead to cone fracture can be found at the bottom of the anchor bolt. In addition, adhesive fracture was confirmed in the concrete area with a depth of 10 to 15 mm around the anchor bolt. Regarding the adhesive stress distribution, it was found that the stress decreased to zero at the bottom and at about 10–15 mm depth of the concrete. This phenomenon indicate that the bond stress can be influenced by cracks. At the upper part, the constraint from the surrounding concrete is relatively low. Micro cracks and major radial cracks can both be found in this area. Thus, the bond stress in this area decreases at an earlier stage [12,15].

In Figure 12c,d, where the adhesive stress limit is 12 MPa, crack development and bond stress distributions are similar to the previous case. With the increase of adhesive stress limit, the cone area at the upper part of the anchor bolt when $x = 225$ μm is larger than that in Case 1. The final fracture pattern changed from bond fracture to bond-cone complex fracture. In Figure 12e,f, where the bond stress is 16 MPa, the crack development and the bond stress distribution of $x = 75$ μm is similar to previous cases. When $x = 300$ μm, the crack reaches the surface of the concrete block, and the bond stress on the lower part of the anchor bolt decreases, forming a cone shaped fracture pattern.

The load-displacement relationship of Case 1, 2, and 3 is shown in Figure 13, where it shows that, with the increase of the maximum bond stress, the maximum load is increasing. For the case with bond stress of 8 MPa where the fracture pattern is bond fracture, the shape of the load-displacement curve is similar to the bond-stress curve mentioned in Figure 3b. For the case with bond stress of 12 MPa where the fracture pattern is compound fracture, it can be found that the area of the load-displacement curve is larger than the previous curve, indicating that the energy consumed in compound fracture is larger than in bond fracture. For the case with bond stress of 16 MPa, the maximum load is larger than the previous cases, and the area of the load-displacement curve, or the energy consumed, is even larger. Because of concrete cracks generated in this process, more noise can be observed in the curve.

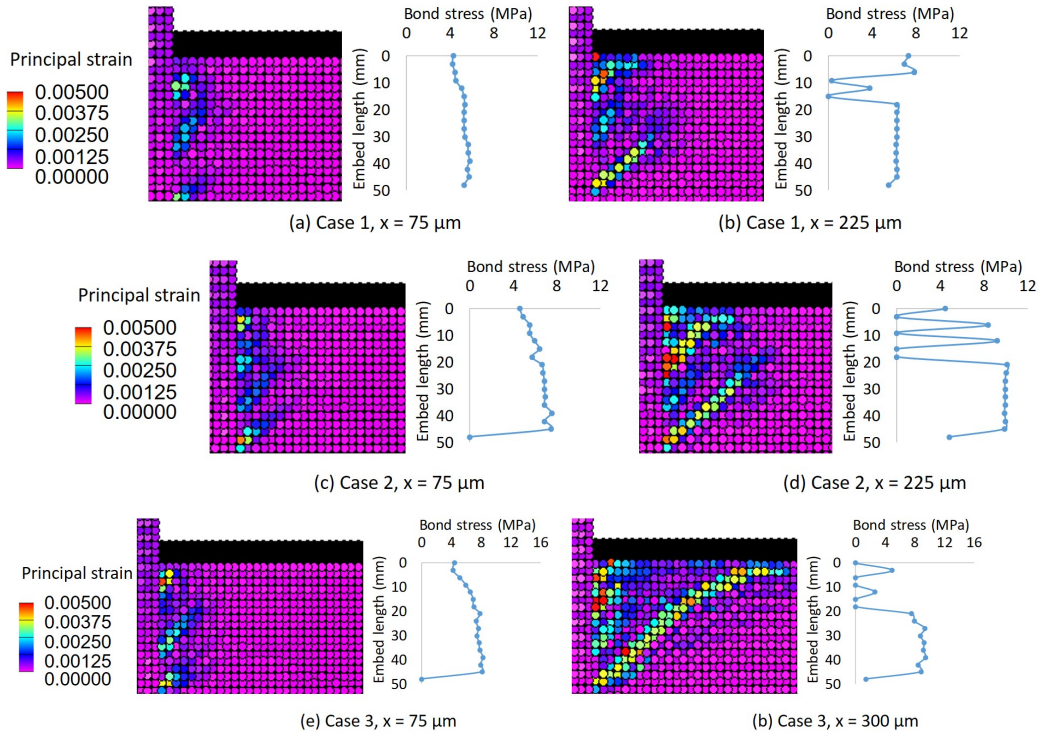

Figure 12. Crack development and bond stress distribution. (**a**,**b**) Case 1. (**c**,**d**) Case 2. (**e**,**f**) Case 3.

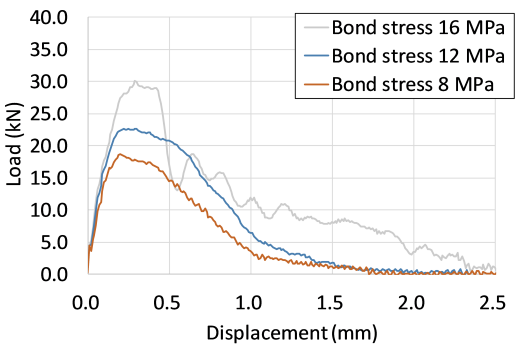

Figure 13. Load-displacement relationships with different bond stress.

For case 2, 6, and 7, when increasing the diameter of the anchor bolt, the damage pattern changed from bond damage to cone damage, shown in Figure 14, and the load-displacement relationship is shown in Figure 15. When the diameter of the anchor bolt increases, more bond force is provided by the increased interface area between anchor bolt and concrete. This bond force is subjected to the same amount of concrete in a cone-shaped area; thus, more concrete is damaged with more bond force by the pull-out process.

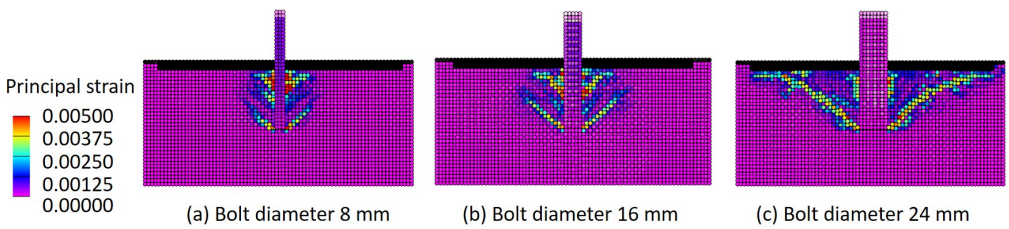

Figure 14. Effect of anchor bolt diameter on the fracture pattern.

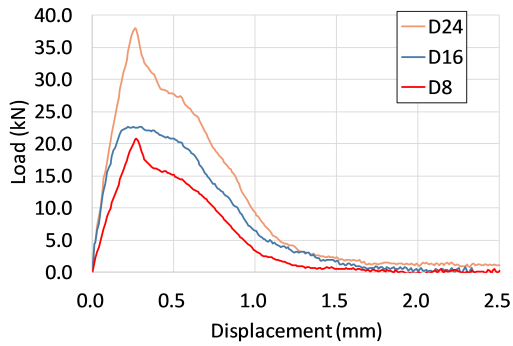

Figure 15. Load-displacement relationships with different anchor bolt diameters.

For case 2, 4, and 5, when changing the embedment depth of the anchor bolt from shallow to deep, the damage pattern changed from cone damage to bond damage, shown in Figure 16, and the load-displacement relationship is shown in Figure 17. When the embedment depth of the anchor bolt increases, the volume of the cone-shaped area also increases. Although more bond force is provided by the increased interface area, the fracture pattern changes from cone fracture to bond fracture due to more concrete participating in resisting the bond force.

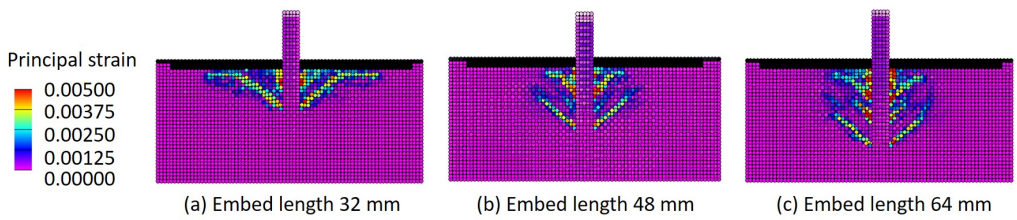

Figure 16. Effect of embedment depths on the fracture pattern.

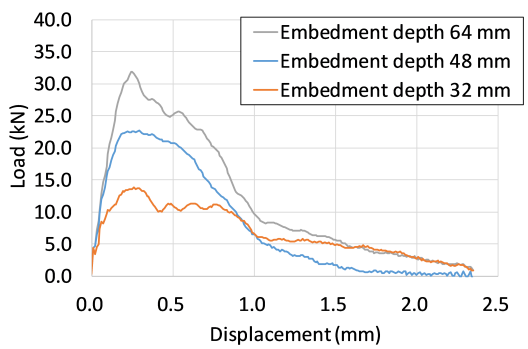

Figure 17. Load-displacement relationships with different embed depths.

To summarize, the analysis cases with bond stress of 12 MPa and their final crack pattern are listed in Table 5 and Figure 18. In this figure, the horizontal axis is the ratio between embedment depth l_e and the anchor bolt diameter d, while the vertical axis is the maximum load P in the pull-out process. When $l_e/d < 3$, the fracture pattern is cone fracture; when $l_e/d > 3$, the fracture pattern is bond fracture; and, when $l_e/d = 3$, the fracture pattern is cone-bond complex fracture. This figure shows the tendency that, in this study, with the increase of the value of l_e/d, the fracture pattern changes from cone fracture to bond fracture.

Table 5. Analysis cases and final crack pattern.

Case	Maximum Bond Stress (MPa)	Anchor Bolt Diameter (mm)	Anchor Bolt Embedment Depth (mm)	Final Crack Pattern
2	12	16	48	Bond-cone complex fracture
4	12	8	48	Bond fracture
5	12	24	48	Cone fracture
6	12	16	32	Cone fracture
7	12	16	64	Bond fracture

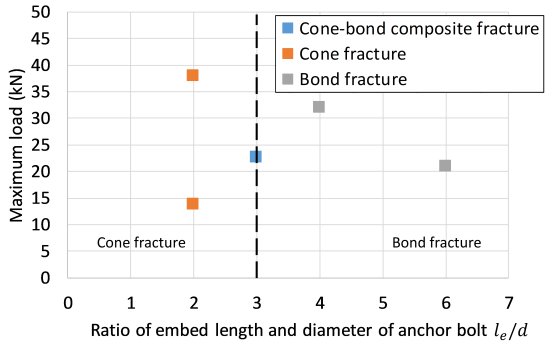

Figure 18. Classification of the pull-out fracture pattern of an anchor bolt.

4.3. Influence of the Spacing between Anchor Bolts

Then, the influence of spacing between anchor bolts to the load capacity of the anchor bolt is investigated. The analysis model is shown in Figure 19, with different spacing between anchor bolts s, from 234 mm to 25 mm. The sides of the upper surface of the concrete block are fixed, and the material parameters are the same with previous analysis. The development process of the cracks during the pull-out process is shown in Figures 20–22.

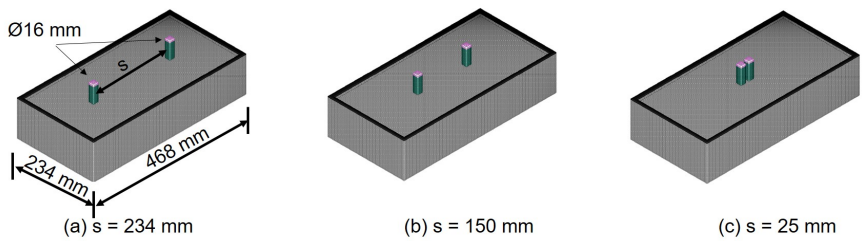

Figure 19. Analysis model with different spacing.

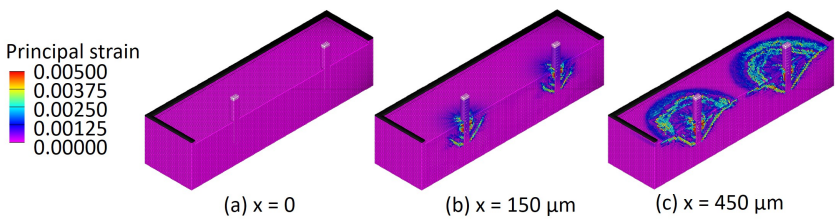

Figure 20. Crack development when the spacing s is 234 mm.

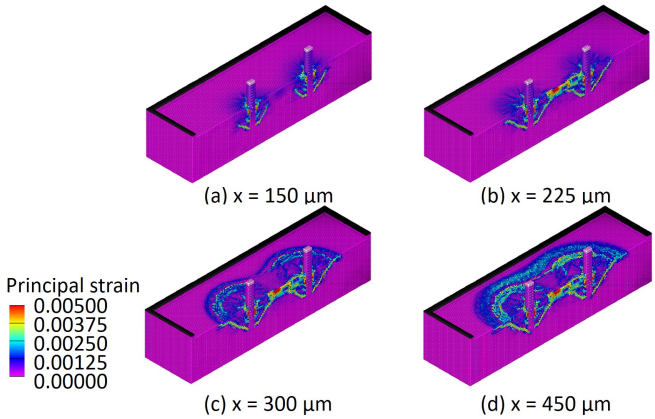

Figure 21. Crack development when the spacing s is 150 mm.

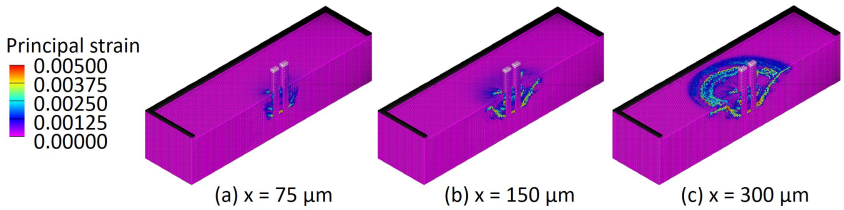

Figure 22. Crack development when the spacing s is 25 mm.

In the case where the spacing is 234 mm, the development process is similar to the case with a single anchor bolt. Inclined cracks generate from the bottom of the anchor bolt and, finally, reach the surface of the concrete block. Two separate cone areas are formed. When the spacing s is 150 mm, the inclined cracks also generate at the bottom of the anchor bolt. When the pull-out displacement $x = 225$ µm, the cracks located between the two anchor bolts joint with each other, forming a long crack connecting the two anchor bolts. When $x = 300$ µm and $x = 450$ µm, the cracks reach the surface of the concrete, and a complicated double-cone fracture surface is obtained. When the spacing s is 25 mm, cracks generate from the bottom of the anchor bolt. The cracks outside the anchor bolts are long and inclined, and the cracks between the anchor bolts are short and horizontal. When $x = 225$ µm and $x = 300$ µm, the inclined cracks reach the surface of the concrete block. The shape and the area of the emerged cone shape becomes more like the cone shape of a single anchor bolt.

The load-displacement curves are shown in Figure 23. In the case where the spacing s is 150 mm, the total area of the emerged cone shape changed little compared to the two separate cone shapes, and the maximum load remains same for spacing of 200 mm and 150 mm. When the spacing s is 25 mm, the two anchor bolts just behave as a single anchor bolt, and the maximum load is about half of the previous cases. To make the tendency more clear, relationship between the ratio between the total maximum load and the maximum load of a single anchor bolt P_{total}/P_{single} and the spacing s is shown in Figure 24a, and the relationship between the ratio between the total maximum load and the maximum load of a single anchor bolt P_{total}/P_{single} and the ratio between spacing and embedment depth s/l_e is shown in Figure 24b. In Figure 24a, it is found that the maximum load remains unchanged when the spacing s is larger than a certain value in different case, which is also described in Reference [28]. In Figure 24b, it is clear that the load decrease is not noticeable until s/l_e reaches 2.0. Compared to existing studies that considered the effect of anchor bolt diameter on sufficient embedment depth [28], this study investigated the effect on pull strength of adjacent bolt spacing at relatively shallow embedding depths. As a result, it is confirmed that an interval of 2.0 times of the embedment depth is needed as a minimum distance of adjacent bolt spacing to keep the pull-out strength. This result indicates that a

minimum spacing of 2.0 times of the embedment depth should be ensured for anchor bolts to provide sufficient resistance against pull-out load.

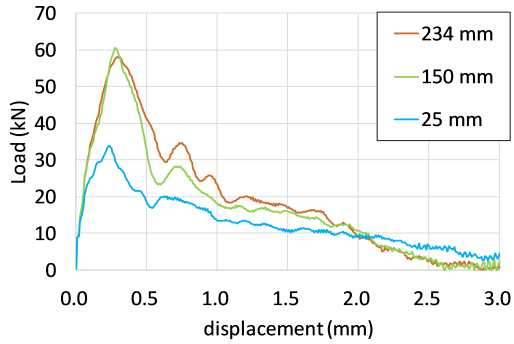

Figure 23. Load-displacement relationships with different spacing.

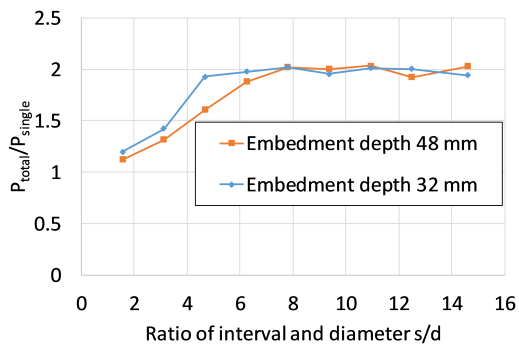

(**a**)

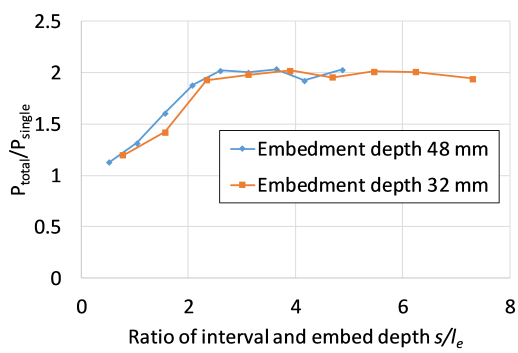

(**b**)

Figure 24. Pull-out strength influenced by input parameters. (**a**) Effect of bolt spacing on pull-out strength (compared to the strength of a single bolt). (**b**) Effect of embedded depth on pull-out strength (compared to the strength of a single bolt).

4.4. Influence of the the Distance from Free Edge

The influence of distance between the edge of the concrete block and the anchor bolt is investigated. The analysis model is shown in Figure 25. The embedment depth l_e is 48 mm, and distance s between the edge of the concrete and the anchor bolts varies from 100 mm to 17 mm. As a boundary condition, the vertical displacement of the black color area (along 3 sides) in the upper surface are fixed, and the other side is not fixed. Figure 26 show the principal strain distribution in half the region of the analysis model in consideration of mechanical symmetry under the 0.45 mm pull-out displacement level.

From the final crack pattern, it was found that, when there is enough distance from the edge of concrete block, a cone-shaped crack pattern can be observed. However, the cone-

shaped crack becomes incomplete with the decrease of distance s. In particular, the crack at the bottom of the anchor bolt extended to the lateral surface of the concrete without changing direction in the case of $s/l_e = 0.4$, while, in other cases, the cracks turned. From the load-displacement relationship shown in Figure 27 and the relationship between the maximum load and the ratio of distance to free edge and embedment depth s/l_e shown in Figure 28, it can be recognized that the maximum pull-out strength decreased when s/l_e is lower than 1.0, and the maximum pull-out strength in case of $s/l_e = 0.4$ decreased around 40% compared with other cases. As a reference, about 50% of the maximum load drop can be found in the experiment [8,16]. Compared to the existing studies [8] that showed the influence of the anchor bolt diameter under sufficient embedment depth, we investigated the minimum distance from the free end to keep the pull-out strength of the anchor bolt, and it has been found that maintaining proper pull-out strength requires a distance from the free end that is greater than 1.0 times the anchor bolt embedding depth. This is also shown by the tendency of the experiments conducted in Reference [16]. Thus, it indicates that $s/l_e = 1.0$ should be guaranteed when installing anchor bolts at the edges of the concrete structures. In addition, compared to the analysis results in the previous section, it can be found that the analysis model with insufficient distance between the anchor bolt and the free edge is similar to a half model of cases with insufficient intervals between anchor bolts considering symmetricity. When sufficient valid base concrete around a single anchor bolt is not guaranteed, the pull-out performance of this single anchor bolt is limited. When installing anchor bolts under these conditions, it is necessary to avoid densely placed rebar areas to ensure sufficient embedding depth for the bolts and the surrounding concrete area. In the next section, we will consider an example of countermeasures when a sufficient concrete area cannot be secured around the anchor bolt.

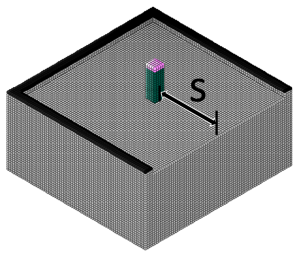

Figure 25. Analysis model with one side free.

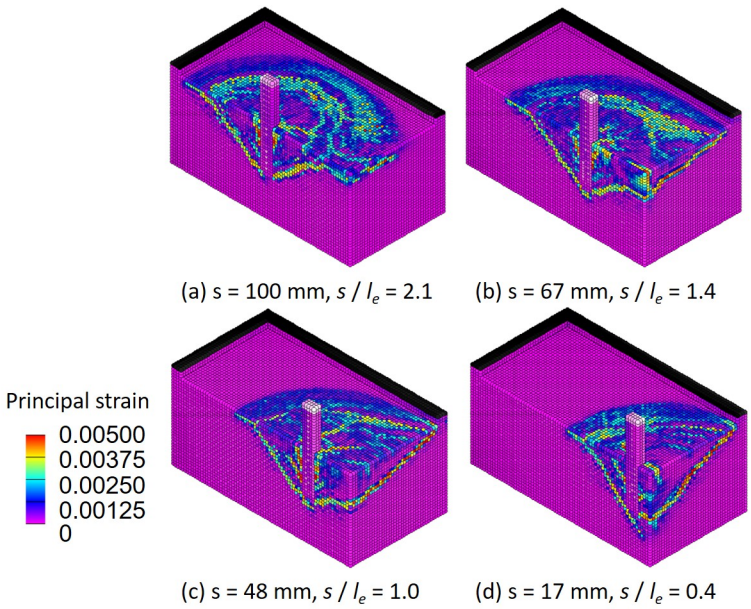

Figure 26. Crack patterns with different distance between the free edge and the anchor bolt.

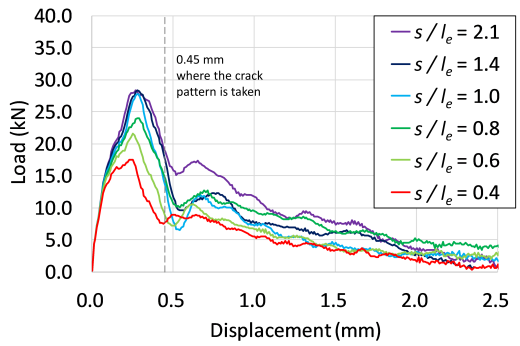

Figure 27. Load-displacement relationships with different distance to free edge.

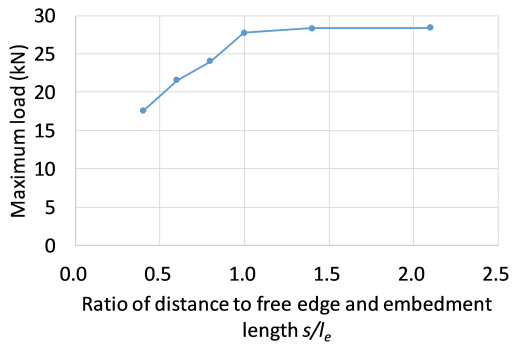

Figure 28. Relationship between maximum load and ratio of distance free edge and embedment depth s/l_e.

4.5. Measures against Insufficient Distance from the Free End with PCM

As clarified in the previous section, if the anchor bolt installation position is close to the free end, the pull-out strength will decrease. We investigated a method that does not reduce the pull-out strength as much as possible, even when anchor bolts are unavoidably attached near the free end by using PCM (Polymer Cement Mortar).

PCM is a simple method of spraying reinforced mortar onto the existing concrete of an aged RC structure, and it has already been used in many ways [23,24]. In this study, we calculated how much the anchor bolt pull-out strength can be prevented from decreasing by PCM method when the anchor installation position is close to the free end.

The analysis model of this simulation is shown in Figure 29, where a PCM reinforcement layer with 3-mm or 6-mm thickness is added to the existing concrete surface. In Figure 29a, the PCM area is smaller, but it is able to cover the projection of the anchor bolt on the lateral surface of the concrete block, while, in Figure 29b, the PCM area is sufficient to cover sufficient the corn failure domain. The material parameters of PCM is shown in Table 6. The boundary conditions are the same as the previous section, where the three sides of the upper surface displayed in black in the figure are fixed.

Figure 30 shows the crack pattern obtained in SPH analysis, and Figure 31 shows the load-displacement relationship. It is recognized from Figure 30a,b that, since the strength of the PCM material is higher than that of existing concrete, the cracks can be seen growing under the PCM area. Thus, this change in the crack growth path causes a slight increase in the pull-out strength of the anchor bolt.

On the other hand, in the case of Figure 30c,d, when the PCM reinforcement area is wide, a crack occurred in the PCM layer, which has a high tensile strength than that of existing concrete, and a clear effect was seen, such as an improvement in pull-out strength of about 40%. To summarize these results, it is possible to improve the pull-out strength of anchor bolts with insufficient distance from free end by using the PCM method. To achieve a better performance of the PCM reinforcement layer, the reinforced area by PCM should be large enough to cover the assumed cone failure domain of the concrete.

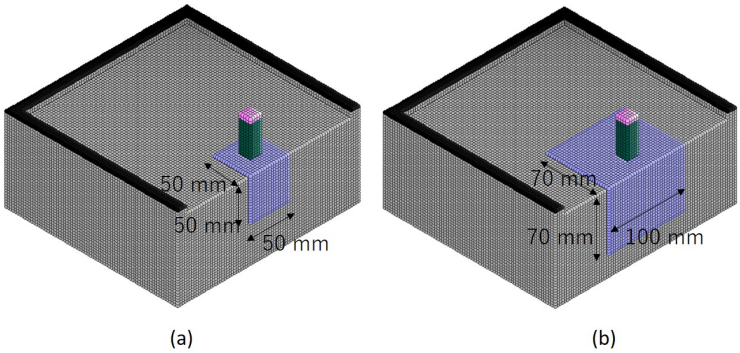

Figure 29. Analysis model with PCM reinforcement layer. (**a**) Model with PCM layer of small area. (**b**) Model with PCM layer of large area.

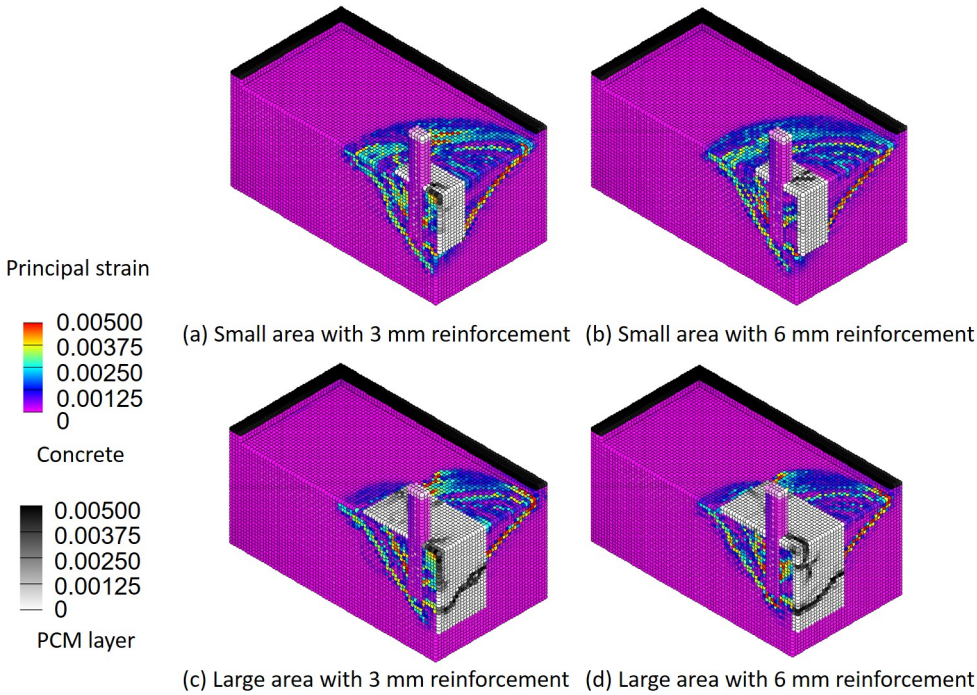

Figure 30. Crack patterns with PCM reinforcement layer.

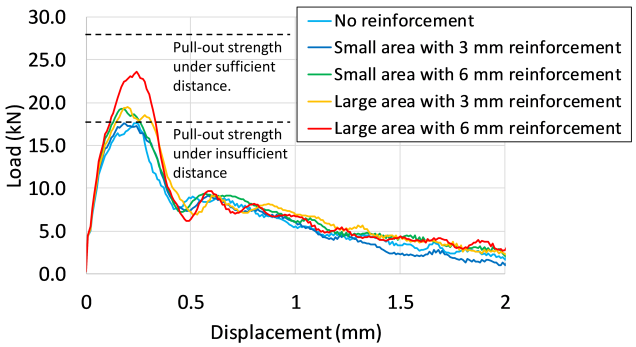

Figure 31. Load-displacement relationships with PCM reinforcement layer.

Table 6. Material parameter of PCM.

Compressive Strength (MPa)	Tensile Strength (MPa)	Poisson's Ratio	Density (kg/m^3)	Young's Modulus (MPa)
60.0	6.0	0.2	2300	27,000

5. Conclusions

In this study, an analysis method that can accurately evaluate the pull-out strength of anchor bolts embedded in concrete using the SPH method is presented and considered the ultimate pull-out strength under various conditions (bolt diameter, embedded depth, adjacent bolt spacing, etc.). The results obtained in this study are summarized as follows.

1. As a result of comparison with the existing experimental values, it was confirmed that the crack growth analysis using the SPH method proposed in this study was very effective on the accurate estimation of ultimate pull-out strength of anchor bolt.
2. When changing the parameters of the analysis cases, concrete base fractures are likely to occur with lower embedding depth and higher bond stress, and bond fractures are likely to occur with deeper embedding depth and lower bond stress.
3. It was found that, if the distance between two adjacent bolts was shortened under the installation conditions where cone fracture occurred, the cone fracture regions of the individual bolts overlapped, and the total pull-out strength of the two bolts decreased. According to the analysis results, if the distance between two adjacent bolts was smaller than embedded depth, the total pull-out strength decreases around 50% compared to the sufficient distance condition.
4. It was also recognized that, when the distance from the edge was larger than the embedment depth, the pull-out strength could maintain the certain level. However, if the distance from the edge becomes smaller than embedded depth, the pull-out strength decreases with the distance.
5. This research simulation shows that, when the distance from the anchor bolt to the edge is about half the embedding depth, the pull-out strength drops to about 50% of the original strength. However, even in such a case, it was confirmed from the analysis results that it is possible to prevent a decrease in the pull-out strength of the anchor bolt by using a PCM material.

In this study, it was shown that the pull-out strength of anchor bolts embedded in concrete could be accurately evaluated by the proposed SPH method. By using this method, it is possible not only to predict the pull-out strength and fracture mode under various installing conditions of anchor bolts in the structure but also to quantify the effect of the reinforcement method, such as the PCM method.

Author Contributions: Conceptualization, Y.S.; methodology, C.L. and Y.S.; software, C.L. and Y.S.; validation, C.L.; formal analysis, C.L.; investigation, C.L. and Y.S.; resources, C.L. and Y.S.; data curation, C.L.; writing original draft preparation, C.L.; writing review and editing, Y.S.; visualization, C.L.; supervision, Y.S.; project administration, Y.S. Both authors have read and agreed to the published version of the manuscript.

Funding: This research received no external funding.

Institutional Review Board Statement: Not applicable.

Informed Consent Statement: Not applicable.

Data Availability Statement: The data that support the findings of this study are available from the corresponding author, upon reasonable request.

Conflicts of Interest: The authors declare no conflict of interest.

References

1. Xiang, N.; Alam, M.S. Comparative seismic fragility assessment of an existing isolated continuous bridge retrofitted with different energy dissipation devices. *J. Bridge Eng.* **2019**, *24*, 04019070. [CrossRef]
2. Yu, P.; Manalo, A.; Ferdous, W.; Salih, C.; Abousnina, R.; Heyer, T.; Schubel, P. Failure analysis and the effect of material properties on the screw pull-out behaviour of polymer composite sleeper materials. *Eng. Fail. Anal.* **2021**, *128*, 105577. [CrossRef]
3. Sharda, A.; Manalo, A.; Ferdous, W.; Bai, Y.; Nicol, L.; Mohammed, A.; Benmokrane, B. Axial compression behaviour of all-composite modular wall system. *Compos. Struct.* **2021**, *268*, 113986. [CrossRef]
4. Yuan, C.; Fan, L.; Cui, J.F.; Wang, W.J. Numerical simulation of the supporting effect of anchor rods on layered and nonlayered roof rocks. *Adv. Civ. Eng.* **2020**, *2020*, 4841658. [CrossRef]
5. Hashimoto, J.; Takiguchi, K. Experimental study on pullout strength of anchor bolt with an embedment depth of 30 mm in concrete under high temperature. *Nucl. Eng. Des.* **2004**, *229*, 151–163. [CrossRef]
6. Munemoto, S.; Sonoda, Y. Experimental analysis of anchor bolt in concrete under the pull-out loading. *Procedia Eng.* **2017**, *171*, 926–933.
7. Richardson, A.; Dawson, S.; Campbell, L.; Moore, G.; Mc Kenzie, C. Temperature related pull-out performance of chemical anchor bolts in fibre concrete. *Constr. Build. Mater.* **2019**, *196*, 478–484. [CrossRef]
8. Yilmaz, S.; Özen, M.A.; Yardim, Y. Tensile behavior of post-installed chemical anchors embedded to low strength concrete. *Constr. Build. Mater.* **2013**, *47*, 861–866. [CrossRef]
9. Epackachi, S.; Esmaili, O.; Mirghaderi, S.R.; Behbahani, A.A.T. Behavior of adhesive bonded anchors under tension and shear loads. *J. Constr. Steel Res.* **2015**, *114*, 269–280. [CrossRef]
10. Nilforoush, R.; Nilsson, M.; Elfgren, L. Experimental evaluation of tensile behaviour of single cast-in-place anchor bolts in plain and steel fibre-reinforced normal-and high-strength concrete. *Eng. Struct.* **2017**, *147*, 195–206. [CrossRef]
11. Eligehausen, R.; Bouska, P.; Cervenka, V.; Pukl, R. Size effect of the concrete cone failure load of anchor bolts. In *Fracture Mechanics of Concrete Structures*; Bažant, Z.P., Ed.; Elsevier Science: London, UK, 1992; pp. 517–525.
12. Bajer, M.; Barnat, J. The glue—Concrete interface of bonded anchors. *Constr. Build. Mater.* **2012**, *34*, 267–274. [CrossRef]
13. Liu, Q.; Chai, J.; Chen, S.; Zhang, D.; Yuan, Q.; Wang, S. Monitoring and correction of the stress in an anchor bolt based on Pulse Pre-Pumped Brillouin Optical Time Domain Analysis. *Energy Sci. Eng.* **2020**, *8*, 2011–2023. [CrossRef]
14. Delhomme, F.; Debicki, G.; Chaib, Z. Experimental behaviour of anchor bolts under pullout and relaxation tests. *Constr. Build. Mater.* **2010**, *24*, 266–274. [CrossRef]
15. Satoh, A.; Takeda, K.; Murakami, K. FEM analysis on combined bond-cone fracture of a post-installed adhesive anchor filled with UHPFRC. *Theor. Appl. Fract. Mech.* **2019**, *100*, 46–54. [CrossRef]
16. Obata, M.; Inoue, M.; Goto, Y. The failure mechanism and the pull-out strength of a bond-type anchor near a free edge. *Mech. Mater.* **1998**, *28*, 113–122. [CrossRef]
17. Soparat, P.; Nanakorn, P. Analysis of anchor bolt pullout in concrete by the element-free Galerkin method. *Eng. Struct.* **2008**, *30*, 3574–3586. [CrossRef]
18. Lu, J.; Zhang, Y.; Muhammad, H.; Chen, Z.; Xiao, Y.; Ye, B. 3D analysis of anchor bolt pullout in concrete materials using the non-ordinary state-based peridynamics. *Eng. Fract. Mech.* **2019**, *207*, 68–85. [CrossRef]
19. Saleem, M. Assessing the load carrying capacity of concrete anchor bolts using non-destructive tests and artificial multilayer neural network. *J. Build. Eng.* **2020**, *30*, 101260. [CrossRef]
20. Lucy, L.B. A numerical approach to the testing of the fission hypothesis. *Astron. J.* **1977**, *82*, 1013–1024. [CrossRef]
21. Libersky, L.D.; Petschek, A.G. Smooth particle hydrodynamics with strength of materials. In *Advances in the Free-Lagrange Method Including Contributions on Adaptive Gridding and the Smooth Particle Hydrodynamics Method*; Springer: Berlin/Heidelberg, Germany, 1991; pp. 248–257.
22. Libersky, L.D.; Petschek, A.G.; Carney, T.C.; Hipp, J.R.; Allahdadi, F.A. High strain Lagrangian hydrodynamics: A three-dimensional SPH code for dynamic material response. *J. Comput. Phys.* **1993**, *109*, 67–75. [CrossRef]
23. Monier, A.; Zhe, X.; Huang, H.; Zhishen, W. External flexural strengthening of rc beams using BFRP grids and PCM. *J. Jpn. Soc. Civ. Eng. Ser. A2 (Appl. Mech. (AM))* **2017**, *73*, I_417–I_427. [CrossRef]
24. Higashi, Y.; Li, B.; Jiang, Y. Reinforcement effect of PCM shotcrete method using FRP grid for tunnel maintenance. In Proceedings of the 2012 International Conference on Renewable Energy Research and Applications (ICRERA), Nagasaki, Japan, 11–14 November 2012; IEEE: Piscataway, NJ, USA, 2012; pp. 1–5.
25. Liu, G.R.; Liu, M.B. *Smoothed Particle Hydrodynamics: A Meshfree Particle Method*; World Scientific: Singapore, 2003.
26. JSCE (Japan Society of Civil Engineers). *Standard Specifications for Concrete Structures: Design*; JSCE: Tokyo, Japan, 2012; pp. 37–38.
27. Popovics, S. A numerical approach to the complete stress-strain curve of concrete. *Cem. Concr. Res.* **1973**, *3*, 583–599. [CrossRef]
28. Eligehausen, R.; Cook, R.A.; Appl, J. Behavior and design of adhesive bonded anchors. *ACI Struct. J.* **2006**, *103*, 822.